UNCLASSIFIED

NRL Report 5978

# SHORT-PULSE TECHNIQUES

## PART 1 - KINETICS OF THE TRIIODIDE/IODIDE REACTION ON A PLATINUM ELECTRODE IN NEUTRAL SOLUTION

S. Schuldiner and C.H. Presbrey, Jr.

Electrochemistry Branch
Chemistry Division

August 20, 1963

**U. S. NAVAL RESEARCH LABORATORY**
**Washington, D.C.**

UNCLASSIFIED

CONTENTS


| | |
|---|---|
| Abstract | ii |
| Problem Status | ii |
| Authorization | ii |
| INTRODUCTION | 1 |
| INSTRUMENTATION | 1 |
| Circuitry | 1 |
| Equipment | 2 |
| Procedure | 3 |
| THE TRIIODIDE/IODIDE REACTION | 4 |
| Experimental Procedure | 4 |
| Kinetic Relations | 6 |
| Experimental Results | 10 |
| Discussion | 16 |
| ACKNOWLEDGMENTS | 19 |
| REFERENCES | 19 |

## ABSTRACT

The subject application permits observation of polarization changes on an electrode surface in times as short as 25 nanoseconds. The required miniaturization of the electrolytic cell is achieved by the use of a solion. Short pulses limit electrochemical processes so that only those reactants already present at the metal/solution interface are available for reaction. Kinetic relations for polarization buildup and decay are derived and applied to this redox system for both anodic and cathodic polarization. The variability of the transfer coefficient $\alpha$ found by Newson and Riddiford is confirmed over a wide range in both the anodic and cathodic directions. Kinetic parameters are determined, and the equations based on the Vetter electron transfer step, with some modifications, are verified. Surface coverage determinations indicate that the fraction of available platinum surface covered with adsorbed iodine atoms at zero overvoltage is 0.09. Parameters are also determined for the hydrogen formation reaction at potentials where all of the iodine is reduced. A model for the adsorption of iodine species on the electrode surface is given in order to explain the relationship between surface coverage of these species and the exchange current density.


## PROBLEM STATUS

This report is on one phase of the problem of electrode mechanisms. Additional work on this problem is continuing.

## AUTHORIZATION


NRL Problem C05-13
Project RR 001-01-42-4754

Manuscript submitted June 10, 1963.

# SHORT-PULSE TECHNIQUES

## PART 1 - KINETICS OF THE TRIIODIDE/IODIDE REACTION ON A PLATINUM ELECTRODE IN NEUTRAL SOLUTION

### INTRODUCTION

The object of this investigation was twofold. The first aim was to devise a technique which would allow the determination of transient polarization effects as soon as possible after the imposition or discontinuation of a perturbation. The second aim was to apply such a technique to the study of a redox system.

A solion cell was selected for this work because such a cell physically meets the requirements for polarization measurements at times less than one microsecond after changes are applied to the system. The careful construction of these cells and the purity of the reagents used are also conducive to studies of fundamental reaction kinetics.

### INSTRUMENTATION

#### Circuitry

The basic circuit used in this investigation is the same as that given in an earlier paper (1), with the omission of the horizontal oscilloscope input since these measurements are all made from simple time-base displays. One modified circuit, shown in Fig. 1, was used for very fast pulses having a rise time of 4 nanoseconds. These pulses were used to check for evidence of cell reactions at very short time intervals following the incidence of a pulse. The use of a nominal value of 100 ohms for $R_{std}$ was found to seriously increase the pulse rise time, so this was reduced to 10 ohms, a value sufficient to provide usable current-measurement voltages but not large enough to materially affect the rise time. Furthermore, essentially constant current conditions exist because of the high solution resistance of the cell. The capacitance existing between the reference and the working electrode caused very large overshoot and some ringing on the pulses observed at the reference electrode. The 200-ohm series resistor was used to greatly reduce the overshoot and eliminate the ringing. Higher values of resistance introduced undesirable stray capacitance effects. Since the pulse generator required a nominal 50-ohm load (45 ohms for optimum square-wave pulse shape), it was necessary to shunt the cell circuit with a 68-ohm resistor to provide this load. Thus the internal resistance of the solion cell turns out to be approximately 125 ohms.

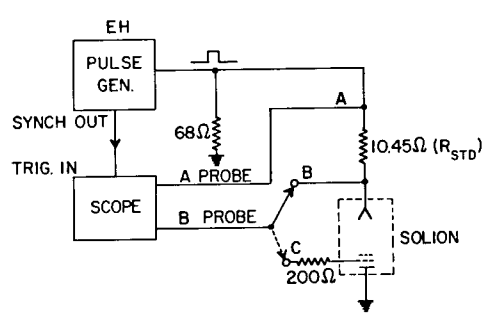


Fig. 1 - Block diagram of the very-short-pulse circuit (pulse rise time: 4 nanoseconds). The generator used was an E-H Model 121 manufactured by E-H Research Labs., Inc.

Since no evidence of cell reactions occurred in the first 25 nanoseconds following pulse incidence, a longer-pulse generator with a pulse rise time of 25 nanoseconds was used with the circuit shown in Fig. 2 for subsequent measurements. The longer rise time eliminated the overshoot and ringing problem, so the 200-ohm resistor shown in Fig. 1 could be omitted and the 10-ohm $R_{std}$ could be increased to the nominal 100 ohms once more, permitting more accurate voltage readings under essentially constant current conditions. Since load matching is not so critical with this generator, the internal 93-ohm load gave a very good wave form with the cell circuit of Fig. 2. Since this generator had a relatively high cutoff current, particularly on the positive output polarity, the four 1N252 diodes were inserted in the cell circuit to hold this down to an insignificant value, as in the former polarization studies (1).

While using the circuit of Fig. 1 with the short-pulse generator, it was decided to check the measurements and calculation method by testing a dummy cell circuit which utilized carefully measured, known values of components. The circuit of Fig. 3 shows the configuration and the values used. Point D was set up to provide a reference pulse for comparison purposes.

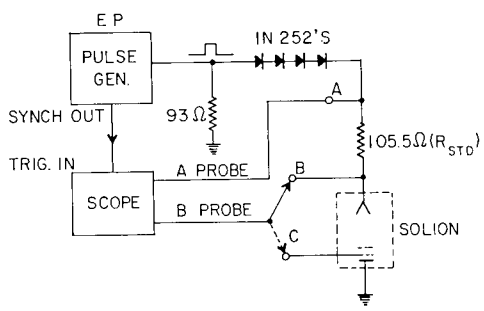


Fig. 2 - Block diagram of the longer-pulse circuit (pulse rise time: 25 nanoseconds). The generator used was the Electro-Pulse Model 3450D manufactured by the Servo Corp. of America.

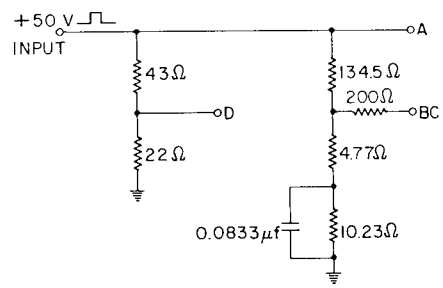


Fig. 3 - RC-cell substitution test circuit used to check the measurements and calculation method for the circuit shown in Fig. 1.

## Equipment

The short-pulse generator used in the circuit in Fig. 1 was the Model 121 manufactured by the E-H Research Labs., Inc. It will supply a ±50v pulse to a 50-ohm load. The pulse rise and fall times are 4 nanoseconds, and the pulse width is variable from 20 to 1000 nanoseconds. Repetition rate is from 10 cycles to 10 megacycles. In addition there is a single-pulse pushbutton.

The long-pulse generator used in the circuit in Fig. 2 was the Electro-Pulse Model 3450D manufactured by the Servo Corp. of America. It will supply a ± 75v pulse to a 100-ohm load. The pulse rise and fall times are 25 nanoseconds, and the pulse width ranges from 50 nanoseconds to 1 second, using two modules. Repetition rate is from 0.05 cycle to 2 megacycles, using two modules. There is also a single-pulse pushbutton.

The oscilloscope used in taking these measurements was a Tektronix Type 585. This is the successor to the Type 535 used in the polarization studies covered by the paper referred to above (1). It is practically identical in its specifications, but it has response up to 100 Mc with a rise time of 3.5 nanoseconds. This response is necessary for use with the short-pulse generator. The dual-trace, switched-input, plug-in amplifier unit

(Type 82) available with this scope was used for the simultaneous display of traces recorded with a Polaroid camera using fast film with 10,000 ASA rating.

The 1N252 diodes are a fast-switching type manufactured by Transitron. They have a maximum inverse operating voltage of 20v, a maximum average forward current of 40 ma, and a maximum recovery time of 0.15 microsecond.

The solion cell used in these studies is described in detail elsewhere in this report, and an enlarged diagram of it is given in Fig. 5.

## Procedure

Initial tests on the solion cell resulted in polarization curves such as those illustrated in Fig. 4. These show the superposition of the pulse at the reference electrode upon the original pulse shape at the very start of the pulse. This is done by means of the electronic switching circuitry contained in the scope preamplifier unit. The three different time bases indicated are used primarily to show the progressive charging of the double layer capacitance over a time in interval of approximately one microsecond. Two Type P6008 probes having a 10-megohm input resistance and 7-pf input capacitance (designed

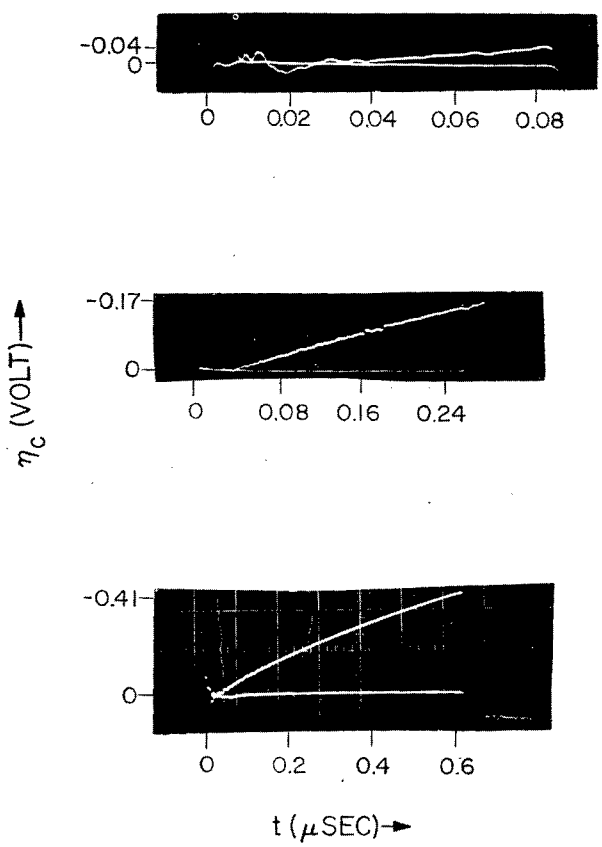


Fig. 4 - Cathodic polarization oscilloscope traces showing electrode overvoltage $\eta_c$ vs time for three different time intervals. The electrode current density was approx. 3 amp/cm$^2$; short-time pulses were used.

specifically for use with the Type 82 plug-in unit) were found to give the best possible wave shape when carefully grounded through BNC connectors to the small shielding box containing the cell. All leads in the box were kept very short to minimize stray inductance and capacitance, and the box was mounted right on the output connector of the pulse generator. The probes were connected to points A and C in Fig. 1, and pulse widths of approximately 0.08, 0.3, and 0.8 μsec were used at repetition rates between 100 and 500 cps. This pulse spacing was sufficient to permit return to equilibrium between pulses. Cell current was obtained by measuring pulse voltages at points A and B with the calibrated scope vertical amplifier. The current is equal to the difference in voltage at points A and B divided by 10.45 ohms.

Similar measurements were made with the long-pulse generator using the circuit of Fig. 2. With the use of pulse widths of 0.8, 8, 45, and 80 μsec, a single-pulse technique was necessary in order to permit the cell to return to equilibrium between the longer pulses. It should be observed that the polarity of the 1N252 diodes must be reversed with a reversal of the input pulse polarity; otherwise their high back resistance will prevent application of the pulse to the cell. The curves in Fig. 6 show positive and negative pulse shapes at the reference electrode. The pulses appear inverted because the actual measurements were taken on the reference electrode (it was necessary to ground the working electrode in arriving at a practical circuit). The curves in Fig. 7, taken in similar fashion, show pulse decay characteristics. With this circuit, the current is equal to the difference in voltage at points A and B divided by 105.5 ohms. This current may be considered constant insofar as its effect on the polarization curves is concerned because the polarization voltage changes are an insignificant proportion of the total applied pulse voltage.

The dummy cell circuit shown in Fig. 3 was assembled in an attempt to approximate the curves obtained from the cell and to calculate the known values of resistance and capacitance by measurements taken from them. In making these measurements, the time base of the scope was carefully calibrated, along with the vertical amplifier voltage calibration. Measurements were taken from pulse photographs obtained by using both pulse generators and pulse polarities. The calculated component values were in reasonable agreement with the measured ones, proving that such measurements are a reliable quantitative source of data when applied to the unknown values in an electrolytic cell.

## THE TRIIODIDE/IODIDE REACTION

Vetter (2,3) reviewed the kinetics of this reaction and concluded that the reaction mechanism would follow the path:

$$I^- \xrightarrow{\text{slow}} I_{ads} + e^- \qquad \text{(electron transfer step)} \quad (1)$$

$$2\, I_{ads} \rightleftharpoons I_2 \qquad (2)$$

$$I_2 + I^- \rightleftharpoons I_3^- \qquad (3)$$

(chemical reaction steps, in equilibrium)

where $I_{ads}$ is a chemisorbed iodine atom. Newson and Riddiford (4) have recently confirmed this mechanism.

### Experimental Procedure

A diagram of the Tracor solion electrical readout integrator is shown in Fig. 5. The solution was reported by the manufacturer to consist of very carefully purified 1.0M KI, plus about 0.0025M $I_2$ and less than 0.01 percent citric acid dissolved in pure water. The cell was constructed of lead-free soft glass in which all the electrodes were sealed inside.

The glass housing was encapsulated in an epoxy potting resin. The oxygen concentration inside the cell was reduced to essentially zero by boiling the solution, out-pumping the gases, and then filling the cell under vacuum. The apparent area of the working electrode was 0.123 $cm^2$, while that of the counter electrode was about 50 times larger. The reference electrode was of the same dimensions as the working electrode, except that to provide an electrolytic path six 0.005-cm holes were equally spaced in a circle midway on the disc, with another hole of the same size in the center of the electrode. The shield electrode shown in Fig. 5 was not used. The temperature of the cell was 25±1°C during the experiment.

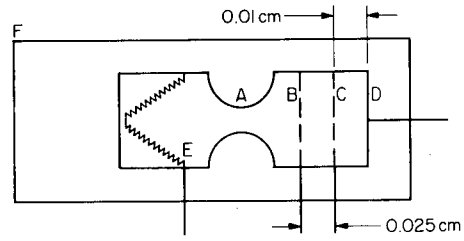


Fig. 5 - Solion electrical readout integrator cell showing (A) cross-section at neck, from 0.05 to 0.1 cm; (B) Pt shield electrode (diam: 0.4 cm) with seven holes of 0.005-cm diam each; (C) Pt reference electrode (diam: 0.4 cm) with seven holes of 0.005-cm diam each; (D) Pt working electrode (diam: 0.4 cm); (E) counter electrode (80-mesh Pt gauze, 0.254 cm by 0.953 cm); and (F) cylindrical plastic case (1 cm diam by 4 cm long) surrounding a glass envelope which contains the electrodes and electrolyte

It was found that when pulses were first applied, polarization was high compared to values obtained when the working electrode was first anodized with a succession of about ten 80-$\mu$sec pulses. This anodizing process undoubtedly cleaned the surface and gave lower polarization results for both anodic and cathodic polarizations. It is possible that this treatment also may have removed any adsorbed citric acid. Indeed, double-layer-capacitance versus overvoltage measurements indicated that no such substance was adsorbed to an important extent on the working electrode surface. The solubility of citric acid in water would also tend to minimize both its rate of adsorption and the amount adsorbed. Measurements were then taken, usually in a period of less than one hour, and in that time the results were reproducible enough so that poisoning effects were not too severe. This was especially true for anodic polarization. Polarization in the cathodic direction, being more subject to poisoning effects, was not as reproducible.

The solion was subjected to single constant-current (varying from 0.1 to 3 amp/$cm^2$) anodic and cathodic pulses of about 0.8, 8, 45, and 80 $\mu$sec duration. The current density was controlled by varying the pulse voltage, and its value was calculated for each pulse from measurements of the voltage drop across $R_{std}$, determined from two pulses usually recorded on the same film with the voltage-time trace for the working electrode. Decay curves were determined by applying single pulses ranging from about 3 to 25 $\mu$sec in duration and recording both the pulse and the potential-time decay trace. Figure 6 shows typical anodic and cathodic single pulses. Figure 7 shows typical anodic and cathodic short pulses followed by decay curves. The rectangular pulses shown on most of these curves were used to determine current density.

The fact that a pulsed working electrode returned to its original open-circuit potential before the application of a succeeding pulse was demonstrated in two ways: first, by photographing a succession of two pulses which coincide upon superposition, and second, by extending the decay time to a point where the decay potential coincided with the potential at the initiation of the pulse. This return to the original open-circuit potential occurred in less than 1000 $\mu$sec. Intervals between successive pulses were of much longer duration. Repeated pulses of a length greater than 80 $\mu$sec caused accumulative effects and some coloration at the anode due to the formation of iodine. However, this condition was carefully avoided during the collection of data.

Open-circuit potentials between each electrode were equal to zero. The calculated equilibrium potential $E_{eq}$ for the triiodide/iodide redox couple is obtained from the following equation.

$$E_{eq} = E_0 + \frac{RT}{2F} \ln \left(a_{I_3^-}/a_{I^-}^3\right) \tag{4}$$

where $E_0$ is the standard equilibrium potential, R is the gas constant, T is the absolute temperature, F is the Faraday, and a is the activity. For the above redox couple, $E_0$ = 0.536 volt (5). For 1M KI and 0.0025M $I_3^-$ the mean activity coefficient of KI is 0.646 (6), and assuming a unit activity coefficient for $I_3^-$, $E_{eq}$ is 0.476 volt. The measured $E_{eq}$ for this solution was reported to be essentially the calculated equilibrium value. The pH of the solution is close to 7. The $I_3^-/I^-$ reaction is apparently at equilibrium at open circuit, so polarization can be represented as an overvoltage. That equilibrium is attained follows also from the findings of Newson and Riddiford (4), who showed that the potential of the triiodide/iodide redox electrode under similar conditions was essentially at its reversible value.

## Kinetic Relations

In this investigation constant current pulses were kept to short durations so that only reactants initially adsorbed on the electrode surface or in the immediate vicinity of the electrode surface would be available for reaction. The transport of iodine or triiodide to and from the electrode is a relatively slow process (2) and hence does not occur significantly during the application of these pulses. Calculations show that the $I_3^-$ concentration in solution at the interface will drop to zero within a few $\mu$sec at the lowest current densities applied. Also the rate of diffusion of $I_3^-$ from the interior of the solution to the electrode surface will be virtually insignificant during the pulse times used. Iodide ion, however, is present in such a relatively large amount that concentration changes of this ion at the electrode interface will be relatively insignificant at the current densities and pulse times used.

The high current density pulses used in this work gave potential-time curves in which the overvoltages were high enough so that the back reaction could be considered to be negligible. The correctness of Vetter's mechanism was assumed, giving the following equations for the rate-controlling anodic and cathodic electron transfer steps, respectively:

$$i_a = i_0 \exp\left(2.3\,\eta_a/b_a\right) \tag{5}$$

$$i_c = i_0\,(\theta/\theta_0) \exp\left(-2.3\,\eta_c/b_c\right) \tag{6}$$

where the subscripts a and c denote anodic and cathodic, carrying respective positive and negative signs, i is the current density, $i_0$ is the exchange current density, $\eta$ is the overvoltage, b is the Tafel slope (= 2.303 $RT/\alpha F$), $\theta$ is the fraction of available platinum surface covered with adsorbed iodine atoms,* $\theta_0$ is the same fraction at zero overvoltage, $\alpha$ is the transfer coefficient, and R, T, and F have their usual meanings. Equation (5) does not contain concentration terms because the iodide ion concentration would be virtually constant for the experimental conditions applied. Changes in surface concentration of adsorbed iodine atoms would be significant in Eq. (6) because of the low concentrations and slow diffusion of $I_3^-$ to the surface.

*Although the adsorbed species will be indicated in the text and figures as iodine atoms, an equivalent of iodine molecules, triiodide ions, or a combination of these may actually exist. More concerning these species will be discussed later.

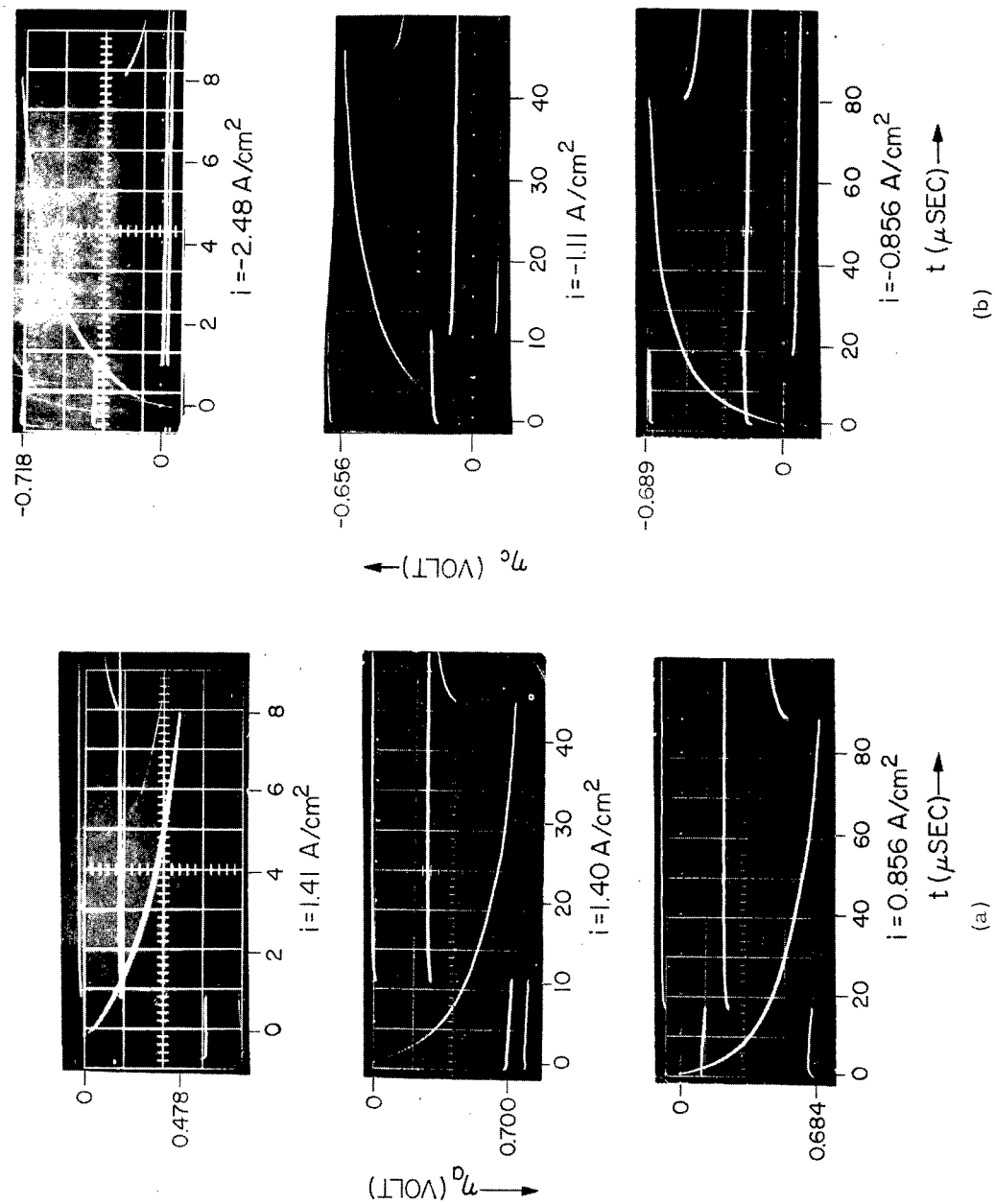


Fig. 6 - Typical polarization oscilloscope traces showing the overvoltage $\eta$ vs time for the working electrode used as (a) the anode and (b) the cathode. The electrode current density i is as indicated. (Note: The two rectangular pulses in each picture were used to determine the current.)

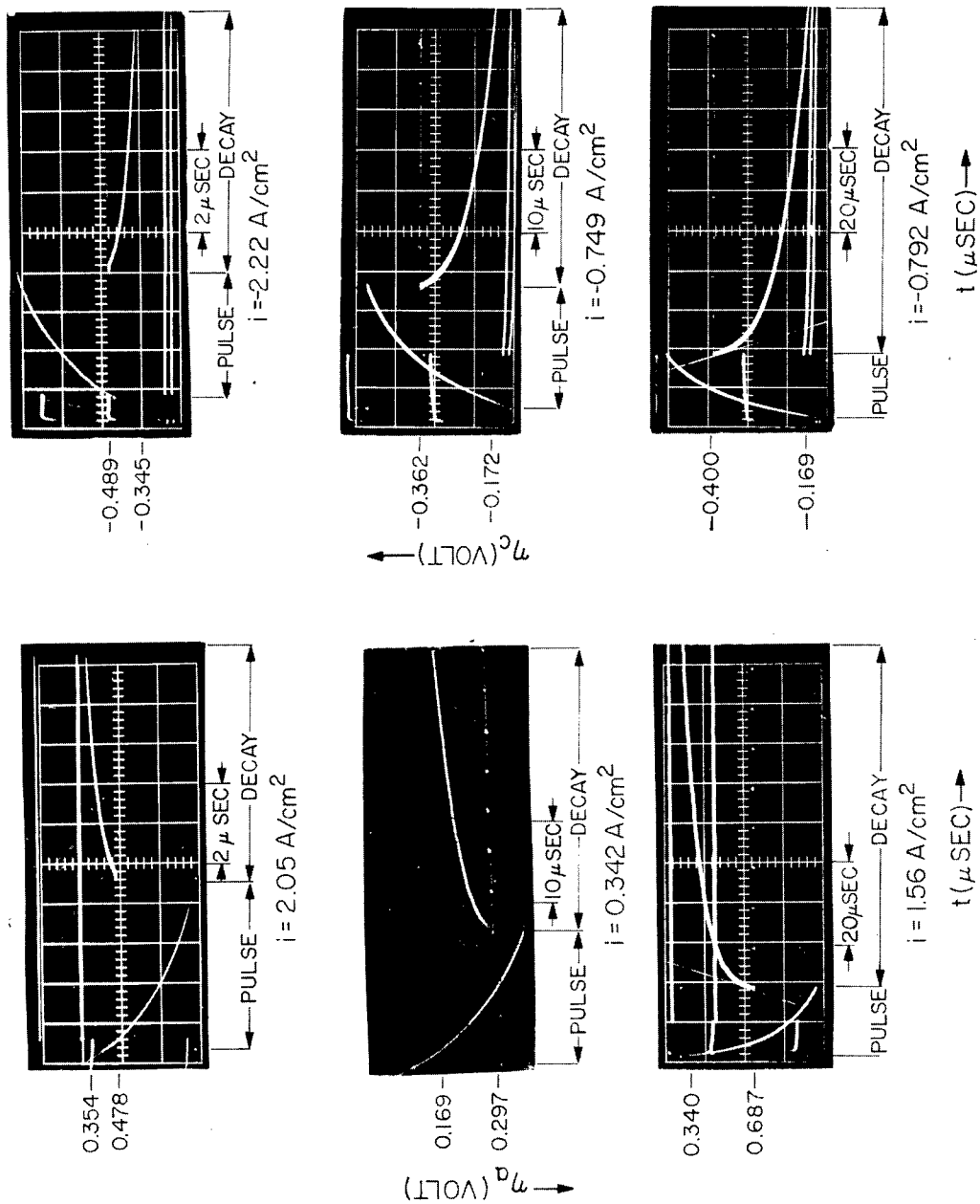


Fig. 7 - Typical pulse and decay oscilloscope traces showing the overvoltage $\eta$ vs time for the working electrode used as (a) the anode and (b) the cathode. The electrode current density i is as indicated. (Note: The two rectangular pulses shown in all but one picture were used to determine the current.)

Transient equations (7,8) were derived for constant current pulse application and also for the decay of potential after the application of a pulse, assuming the simple model of an electrode interface as a double layer capacitance in parallel with a faradaic impedance (the latter being a function of the rate of electron transfer) with no back reaction. Upon polarization with a constant current pulse, and with insignificant concentration changes, the following differential equation describes the rate of overvoltage change:

$$\frac{d|\eta|}{dt} = \frac{|i|}{C} - \frac{i_0}{C} \exp(2.3|\eta|/b), \tag{7}$$

where $t$ is the time and $C$ is the double layer capacitance. Integration of this equation gives

$$|\eta| = \frac{|i|t}{C} - b \log \left[\frac{|i| - i_0 + i_0 \exp(2.3|i|t/bC)}{|i|}\right]. \tag{8}$$

Upon cathodic polarization, where changes in the concentration of adsorbed iodine atoms are significant, Eq. (7) must be modified. Here,

$$\frac{d\eta_c}{dt} = \frac{i_c}{C} + \frac{i_0}{C}\frac{\theta}{\theta_0} \exp(-2.3\ \eta_c/b_c) \tag{9}$$

with

$$\theta = \theta_0 + \frac{N_A \times 10^{-6}\ i_f t}{2 \times 10^{15}\ F} = \theta_0 + 3.125 \times 10^{-3}\ i_f t; \tag{10}$$

$N_A$ is Avogadro's number, $i_f$ is the faradaic current density in amp/cm$^2$, $t$ is time in $\mu$sec, and $2 \times 10^{15}$ is the estimated number of adsorption sites (Pt atoms) per cm$^2$ on the Pt electrode. Also

$$i_c = i_C + i_f, \tag{11}$$

where $i_C$ is the capacitive current density defined by

$$i_C = C\ d\eta_c/dt = C\ \eta_c'. \tag{12}$$

Hence,

$$\theta = \theta_0 + (i_c - C\ \eta_c')3.125 \times 10^{-3}\ t. \tag{13}$$

Substituting Eq. (13) into Eq. (9), we obtain

$$\eta_c' = \frac{i_c}{C} + \frac{i_0\ \theta_0}{C\theta_0 \exp(2.3\ \eta_c/b_c) + 3.125 \times 10^{-3} C i_0 t}. \tag{14}$$

Transient measurements made from potential decay traces after application of a constant current pulse contain important simplifications. This is due to the fact that when the polarizing current pulse is switched off, the current flow through the electrode/solution interface has only a single path. In other words, the double layer capacitance is in series with the faradaic impedance instead of in parallel as in the case of the application of a pulse. This leads to a simplification of Eq. (7):

$$\frac{d|\eta|}{dt} = -\frac{i_0}{C}\exp(2.3|\eta|/b) \quad . \tag{15}$$

Another inherent simplification in decay measurements is that the effects of changes of reactants adsorbed on the electrode surface are canceled out. This is because changes in the number of reactant particles at the time the pulse is switched off affect the exchange current density inversely as these same changes affect potential decay.

Integration of Eq. (15) gives the relation

$$|\eta_0| - |\eta_t| = b \log\left(1 + \frac{2.3|i_i|t}{bC}\right), \tag{16}$$

where $\eta_0$ is the overvoltage at the time the pulse is switched off, $\eta_t$ is the overvoltage at time $t$ after the pulse is switched off, and $i_i$ is the current density of the series arrangement of double layer capacitance and faradaic reaction at the instant after the pulse is switched off. Equation (16) differs from the equation derived by Frumkin (9) inasmuch as in Frumkin's case a constant current was applied until a steady-state voltage was achieved at the electrode. This meant that at current interruption the double layer was fully charged and all of the current flowed through the faradaic impedance. Hence the current density in the series double layer and faradaic impedance at interruption time was equal to the applied current density. In the cases investigated in the present report, steady-state conditions are not reached and the double layer is not fully charged at pulse cutoff time. Hence the current density $i_i$ will be less than the current density applied by the constant current pulse. This is because just after the pulse switchoff time the net current flowing in the series double layer and faradaic impedance will depend on the state of charge of the double layer.

## Experimental Results

The double layer capacitance at open circuit was determined by applying a 0.8-$\mu$sec pulse in both anodic and cathodic directions. The initial slope of the traces was used to determine double layer capacitance from the relation

$$C = i\Delta t/\Delta\eta \quad . \tag{17}$$

For anodic polarization the value of $C$ was 7±1 $\mu$fd/cm$^2$, and for cathodic polarization $C$ was 6±1 $\mu$fd/cm$^2$.

As first demonstrated by Frumkin (9), the relation in Eq. (16) can be used to determine the Tafel slope $b$ from a plot of overvoltage versus log $t$. Tafel $b$ values were found in this manner from all polarization decay traces. Typical overvoltage versus log $t$ decay curves after anodic and cathodic polarization are shown in Fig. 8. These curves show that $b$ is dependent on the total number of coulombs applied in the polarizing pulse. The relation between these quantities is shown in the decay curves of Figs. 9 and 10. The dependence of $b$ on the overvoltage $\eta$ at the time the pulses were switched off is shown in the decay curves of Fig. 11.

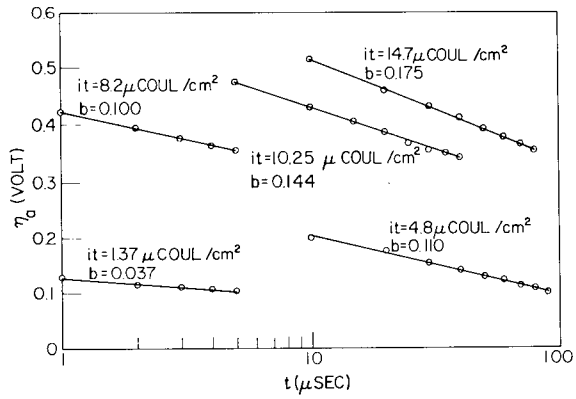


(a)

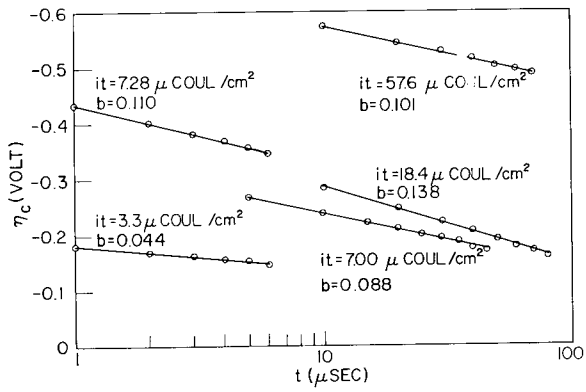


(b)

Fig. 8 - Typical overvoltage ($\eta$) vs log t curves for (a) anodic and (b) cathodic polarization

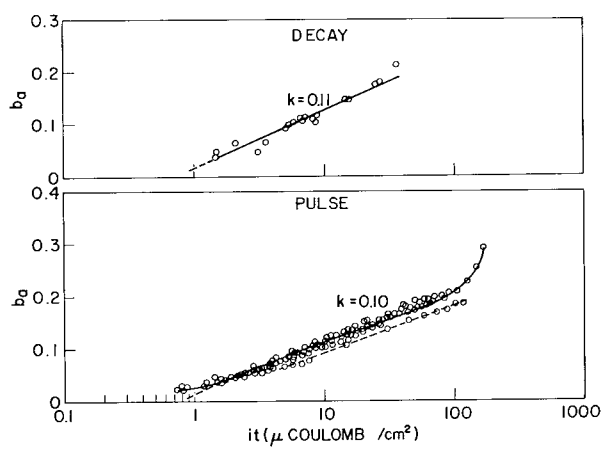


Fig. 9 - Relation between anodic Tafel slope $b_a$ and log it for pulse and decay measurements. The dashed line under the pulse curve shows the data taken from a single pulse.

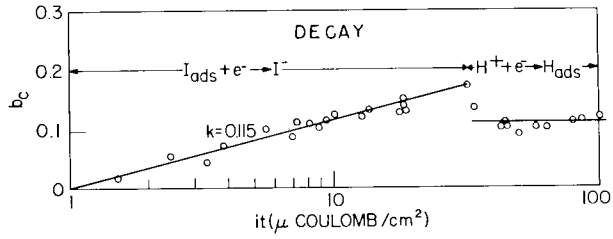


Fig. 10 - Relation between cathodic Tafel slope $b_c$ and log it for decay measurements. The $H^+$ ions indicated in this and other graphs refers to water: $H^+ - O^= - H^+$.

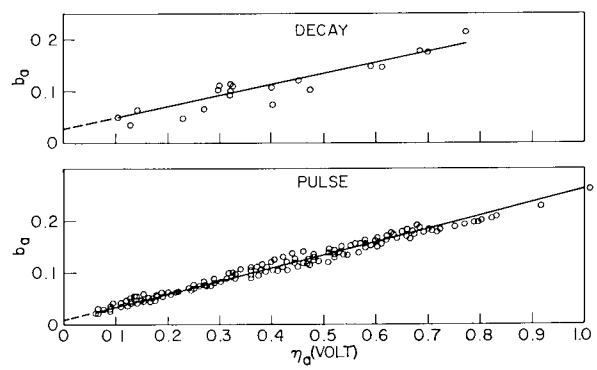


(a)

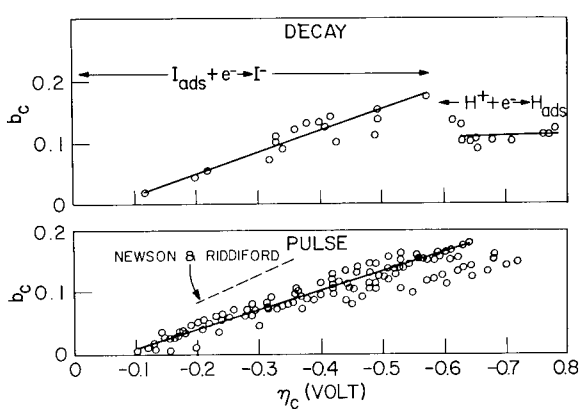


(b)

Fig. 11 - Relation between Tafel slope b and overvoltage $\eta$ for pulse and decay measurements for (a) anodic and (b) cathodic polarization

The decay curves in Figs. 9 and 10 show that during application of a pulse, b is not constant for the $I_3^-/I^-$ reactions but can be expressed by the relation

$$b = a + k \log it, \tag{18}$$

where a is the value of b at $it = 1\,\mu coul/cm^2$, k is the slope of the b versus log it curve and it is the number of $\mu$coulombs per $cm^2$ applied in the polarizing pulse at the time t. This means that Eq. (7) must be modified to

$$\frac{d|\eta|}{dt} = \frac{|i|}{C} - \frac{i_0}{C} \exp(2.3|\eta|/(a + k \log it); \tag{19}$$

or,

$$k = \frac{|\eta|}{\log it \log \left[(i - C|\eta'|)/i_0\right]} - \frac{a}{\log it}, \tag{20}$$

where $\eta' = d\eta/dt$.

The exchange current density $i_0$ was determined from the decay curves by using Eq. (16) to determine $i_i$ and then applying the relation

$$i_0 = i_i \exp(-2.3|\eta_0|/b). \tag{21}$$

These relations are usable because b is determined by the number of coulombs used to polarize the electrode and, as shown in Fig. 8, b remains constant during decay. For anodic decay, a random scatter of the values of $i_0$ was obtained with an average value of $2 \times 10^{-4}$ amp/$cm^2$. Although the scatter was about one order of magnitude, most of the points lay in a reasonable range (0.9 to $2 \times 10^{-4}$ amp/$cm^2$). For cathodic decay, however, the $i_0$ values could not be considered to be constant, and the relation found in Fig. 12 was observed.

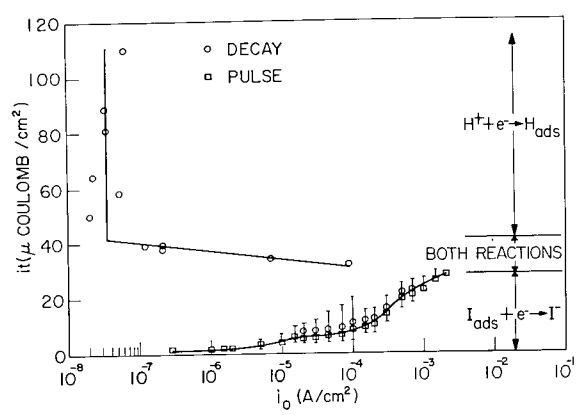


Fig. 12 - Relation between exchange current density $i_0$ and amount of charge for cathodic pulse and decay measurements

Using the average $i_0$ value of $2 \times 10^{-4}$ amp/cm$^2$ found from the anodic decay curves, Eq. (20) was solved for $k$ for discrete experimental values found in the pulse traces. From the $k$ values thus determined, $b_a$ was calculated using the decay curve parameters indicated in Fig. 9 which, upon applying Eq. (18), gave the relation $b_a = 0.015 + 0.11 \log it$. The individual $b_a$ values so determined are shown on the pulse curve in Fig. 9. This latter curve gave the empirical relationship $b_a = 0.015 + 0.10 \log it$. The concordance between the decay and pulse curves shown in Fig. 9 indicates that the kinetic relations used are valid.

Since $i_0$ values were not constant for the cathodic decay curve, it was not possible to run a similar check. Instead, the Eq. (18) relation $b_c = 0 + 0.115 \log it$ found from the decay curve of Fig. 10 was used to determine $i_0$ values for the pulse traces for cathodic overvoltage. This was done for the iodine reduction reaction which terminated at pulse charges above 30 $\mu$coul/cm$^2$. The solution of Eq. (14) for $i_0$ gives

$$i_0 = \frac{\exp(2.3\ \eta_c/b)}{\dfrac{1}{\eta_c'\ C - i_c} - \dfrac{3.125 \times 10^{-3}\ t}{\theta_0}} . \tag{22}$$

The value of $\theta_0$ was determined from Fig. 10, which clearly showed that when more than 30 $\mu$coul/cm$^2$ of charge was applied, all of the adsorbed iodine atoms were ionized and hydrogen ions from water were reduced. This allowed a calculation of the number of iodine atoms adsorbed at open circuit. This was found to be $1.9 \times 10^{14}$ atoms/cm$^2$. Assuming that there are $2 \times 10^{15}$ Pt atoms/cm$^2$ of apparent area of the working electrode, then $\theta_0 = 0.09$. The $i_0$ values determined from the cathodic pulses are shown in Fig. 12 together with the values found from the cathodic decay curves.

Double layer capacitance relationships are shown in Fig. 13. Decay values of capacitance in Fig. 13(a) and 13(b) were determined by multiplying the calculated $i_i$ values for each of the decay oscilloscope traces by the slope $\Delta t/\Delta\eta$ at the beginning of each overvoltage decay. Within the experimental precision, the decay curves indicate that the double layer capacitance is essentially independent of overvoltage. For the cathodic polarization curves, after the application of 30 $\mu$coul/cm$^2$ of charge, the predominant reaction is the reduction of hydrogen ions. In this case $i_0 \approx 3.5 \times 10^{-8}$ amp/cm$^2$ (Fig. 12) and $b = 0.11$ (Figure 10). These parameters show the normal expected behavior of this reaction. Using Eq. (8) and solving for $C$, we obtain the results shown in Fig. 13(b) and 13(c) (pulse curves).

Relationships between the Tafel slope b and overvoltage $\eta$ from the pulse traces are shown in Fig. 11. The relation between the number of iodide ions oxidized or the number of electrons consumed and the overvoltage for the anodic or cathodic pulses, respectively, are shown in Figs. 14 and 15. These measurements were corrected for the number of coulombs used to charge the double layer. The curve marked with X's in Fig. 15 represents the relation between overvoltage and number of hydrogen atoms formed, corrected for the amount of charge used to reduce the iodide ions.

The limits of experimental scatter indicated in Figs. 12, 13(b), 14, and 15 by the vertical lines show the scatter of sets of curves rather than individual points. All points from each individual pulse trace essentially follow the same course as shown by the curve. The curves were drawn through the median of the region of maximum density of individual curves.

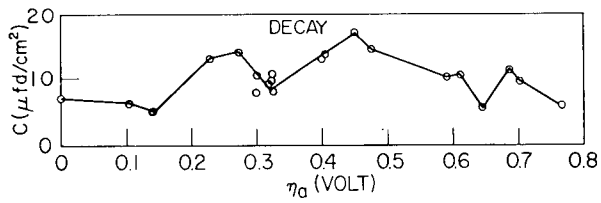


(a)

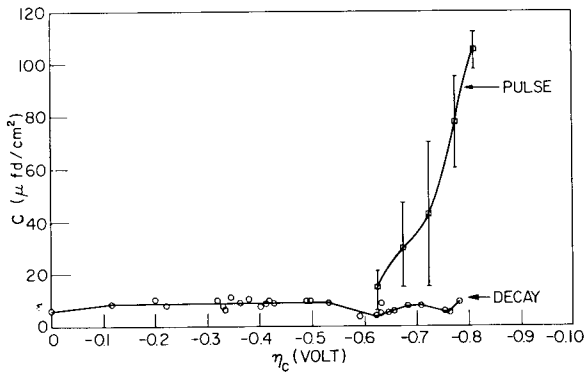


(b)

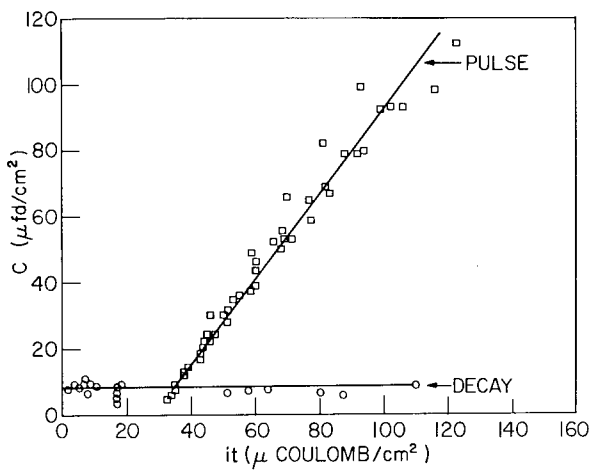


(c)

Fig. 13 - Relation between double layer capacitance and (a) anodic overvoltage at time pulse was switched off, (b) cathodic overvoltage, where $\eta_o$ for decay measurements is the overvoltage at pulse switchoff time, and (c) the amount of cathodic charging for pulse and decay measurements

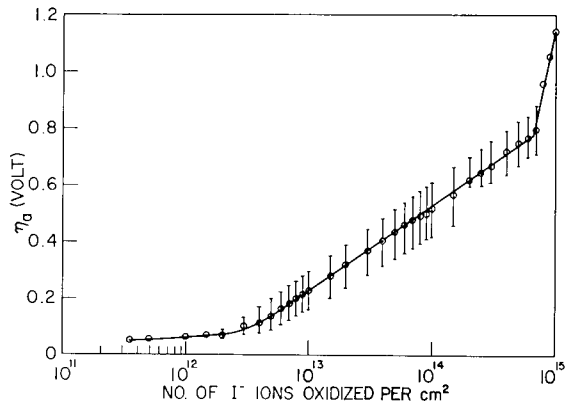


Fig. 14 - Relation between anodic overvoltage and number of $I^-$ ions oxidized per $cm^2$

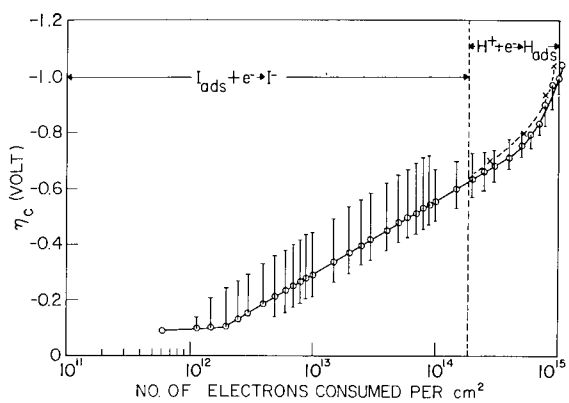


Fig. 15 - Relation between cathodic overvoltage and number of electrons consumed per $cm^2$. Broken line with X's represents relation between number of hydrogen atoms formed and cathodic overvoltage.

## Discussion

The experimental results indicate that the triiodide/iodide reaction is a very complex one and that the simple mechanism shown in Eqs. (1)-(3) is not completely adequate.

Newson and Riddiford (4) found that for cathodically polarized electrodes, the transfer coefficient $\alpha$ was dependent on the bulk concentration of triiodide ion, iodide ion, and the rate of stirring. Their data showing overvoltage dependence was calculated and plotted in Fig. 11(b). One of the interesting results of the present investigation is the indicated dependence of the Tafel slope b on the number of coulombs used to charge the electrode (Figs. 9 and 10) or on the overvoltage (Fig. 11). Thus the transfer coefficient is primarily dependent on the number of adsorbed iodine atoms. The maximum value of $\alpha$ occurs near open-circuit conditions. In this case it can go up to three, an astonishingly high value. Upon either anodic or cathodic polarization, $\alpha$ decreases with either an increase or decrease in the number of adsorbed iodine atoms. In the cathodic direction,

UNCLASSIFIED

when all of the iodine atoms are ionized, the hydrogen formation reaction gives a constant Tafel slope of 0.11 ($\alpha$ = 0.54), as shown in Fig. 10, which is essentially the value expected for this charge transfer reaction.

Newson and Riddiford (4,10) explained the variation of $\alpha$ as due to nonuniformity of the electrode surface, and they postulated that the anodic and cathodic sites differed. This work shows that essentially the same relation holds (see Figs. 9 and 10) for the change in the number of adsorbed iodine atoms and the Tafel slope b in either the anodic or cathodic direction. It is difficult to understand why the transfer coefficient should be so dependent on the concentration of reactant in the cathodic case and on the concentration of product in the anodic case. A relation to the number of active sites, however, seems to be apparent.

With the fast-pulse techniques used (especially at very short times), the mechanisms involved could be different from the steady-state condition represented by Vetter (Eqs. 1-3) since equilibrium of the chemical steps (Eqs. 2 and 3) may not have had enough time to be established. Thus $\alpha$ values greater than one, which were obtained at very short times, may represent a faradaic impedance controlled by the chemical combination/dissociation reaction (Eq. 2) or the complexing of iodine to triiodide (Eq. 3). At longer times, equilibrium could have been established for these steps, and consequently the charge transfer step (Eq. 1) would be rate controlling.

Figure 15 shows that on open circuit there are about $2 \times 10^{14}$ iodine atoms/cm$^2$ adsorbed on the electrode surface. From Fig. 14 it can be seen that when an additional $7 \times 10^{14}$ atoms/cm$^2$ are formed to give a total of $9 \times 10^{14}$ iodine atoms/cm$^2$, a limiting condition is reached, causing a sharp rise in potential. This would indicate that only about one-half the total number of Pt atoms available on the surface are active insofar as the oxidation of iodide ions is concerned. Thus it appears that each adsorbed iodine atom could share bonds with two Pt atoms. This saturation of the active sites with iodine atoms, molecules, and/or triiodide ions indicates also that diffusion away from the surface into the solution is not a limiting factor.

The curves shown in Fig. 13(b) and 13(c) respectively, relate double layer capacitance with cathodic overvoltage and with the number of coulombs/cm$^2$ used to charge the electrode. The decay curves in both figures show only minor variation, whereas the pulse curves show a sharp rise at the point where formation of adsorbed hydrogen atoms becomes the predominant reaction. The fact that the rise in capacitance occurs only during pulsing can be due to the removal of iodine atoms which act as an electrode poison and tend to lower the capacitance. The low capacitance found for decay curves, even in the range where the predominant reaction before pulse cutoff was the formation of hydrogen, indicate that removal of the polarizing current was accompanied by readsorption of enough poison to lower the double layer capacitance even though part of the reaction during pulse decay may still be the formation of hydrogen atoms. The absence of capacitance peaks in all of the double layer capacitance curves, other than that for the hydrogen formation reaction, indicates also that citric acid was not adsorbed on the working electrode.

The fact that exchange current density on anodic polarization showed no dependence on the number of coulombs used to charge the electrode is expected since the concentration of $I^-$ ions remains effectively constant. A very strong dependence is indicated for the cathodic case, as Fig. 12 shows. For small changes in the amount of charge, the exchange current density increases very rapidly with the amount of charge. A reduction in the rate of change of $i_0$ with charge is evident at about 10 $\mu$coul/cm$^2$. At 30 $\mu$coul/cm$^2$ the adsorbed iodine is virtually completely removed and the exchange current density drops off very rapidly as the hydrogen formation reaction takes over. Eventually the hydrogen reaction dominates, to give an essentially constant $i_0$ for this reaction at about $3.5 \times 10^{-8}$ amp/cm$^2$. The increase in $i_0$ in the range of the iodine reaction is accompanied by a very rapid decrease in the number of iodine atoms available for reaction. This

increase in $i_0$ is surprising since $i_0$ is a direct function of concentration and, therefore, the opposite effect would be expected. This can only mean that the activation energy for the reduction of adsorbed iodine atoms decreases as the number of iodine atoms decreases. Since the activation energy term in the kinetic equation is an exponential, the effect of lowered activation energy overwhelms the effect of lowered concentration of reactant.

The determination of $i_0$ for anodic and cathodic polarization does not necessarily indicate the $i_0$ which would be found near open circuit. It appears that $i_0$ at $\eta \to 0$ would be small. Thus at short times very little current would flow in the faradaic arm; this results in a rapid rise in the potential primarily due to the charging of the double layer. The maximum $i_0$ value of $2 \times 10^{-3}$ amp/cm$^2$ found for the cathodic iodine reduction reaction (see Fig. 12) would be the effective exchange current density for the electron transfer step under steady-state cathodic polarization, where the rate of the reaction is controlled by the diffusion of triiodide ion to the electrode surface.

In this report we have in a general way referred to the adsorbed reactant on cathodic polarization as iodine atoms, without specifying how these atoms were associated on the surface. The adsorption can be visualized as

```
                I⁻          I⁻          I⁻
                +          / \          +
I   I ⇆ I - I ⇄ I   I ⇄ I   I
|   |   |   |   |   |   |   |
Pt  Pt  Pt  Pt  Pt  Pt  Pt  Pt
```

where an equilibrium between iodine atoms, molecules, and triiodide ions is visualized. The concentration of each of these species on the surface is not known, although it is quite likely that the triiodide ion dominates. The increase in $i_0$ as the concentration of these reactants decreases from the open-circuit value of $\theta_0 = 0.09$ may be due to a large increase in the heat of adsorption of the chemisorbed species. The evidence of Vetter (2) and Newson and Riddiford (4) indicates that the reduction of the adsorbed species is a one-electron step. However, the reduction may take place from any one or all of these species. As the electrode becomes more negative, the bonds between the iodine atoms and the iodide in the triiodide ion could be weakened due to repulsion of the iodide. This would tend to favor the formation of either adsorbed iodine atoms or molecules. This could also favor the direct reduction of triiodide ions.

Upon anodic polarization, the surface is undoubtedly largely covered with adsorbed iodide ions (11,12). Thus the effective concentration of reactant remains relatively constant, as indicated by the independence of the exchange current density from the amount of charge passed. The additional coverage of the surface with iodine atoms, molecules, and triiodide ions at increasing polarization does not materially affect the activation energy for the oxidation of iodide ions. Effects of the back reaction are negligible at the overvoltages obtained.

This investigation has demonstrated the effectiveness of the short-pulse technique when used to obtain information concerning a very complex electrode process. Much more work is indicated in order to clarify the many complex features of the triiodide/iodide system.

ACKNOWLEDGMENTS

We are indebted to Dr. Ray M. Hurd of Tracor, Inc., for furnishing the integrator solion used in this study and for the information he gave concerning the construction and properties of this cell. We gratefully acknowledge the assistance of Mrs. Janet P. Mason* in making computations on the Naval Research Laboratory digital computer (NAREC) and the professional aid of Dr. H.A. Hauptman.*

## REFERENCES

1. Presbrey, C.H., Jr., and Schuldiner, S., J. Electrochem. Soc. 108:985 (1961)
2. Vetter, K.J., Z. physik. Chem. 199:22, 285 (1952)
3. Vetter, K.J., "Elektrochemische Kinetik," p. 374, Berlin:Springer Verlag, 1961
4. Newson, J.D., and Riddiford, A.C., J. Electrochem. Soc. 108:699 (1961)
5. Latimer, W.M., "The Oxidation States of the Elements and Their Potentials in Aqueous Solutions," 2d ed., p. 64, Englewood Cliffs, N.J.:Prentice-Hall, 1952
6. Harned, H.S., and Owen, B.B., "The Physical Chemistry of Electrolytic Solutions," 3d ed., p. 731, New York:Rheinhold, 1958
7. Roiter, V.A., Yuza, V.A., and Poluyan, E.S., Zhurn. Fiz. Khim. 13:605, 805 (1939)
8. Kheifets, V.L., and Sheinin, A.B., Russ. J. Phys. Chem. 33:233 (1959)
9. Frumkin, A.N., Acta Physicochim. USSR 18:23 (1943)
10. Ledger, W.A., and Riddiford, A.C., Nature 194:1233 (1962)
11. Frumkin, A.N., and Aikazyan, E.A., Dokl. Akad. Nauk USSR 100:315 (1955)
12. Shanina, L.T., Dokl. Akad. Nauk USSR 134:141 (1960)

*Applied Mathematics Staff, NRL.